# Plasma-made (Ni$_{0.5}$Cu$_{0.5}$)Fe$_2$O$_4$ nanoparticles for alcohol amination under microwave heating
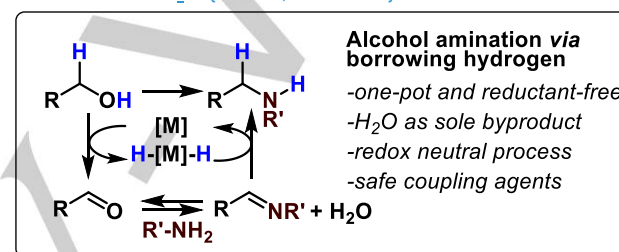
Alain You Li[a] † and Nicolas Dumaresq[b] †, Andréanne Segalla[a], Nadi Braidy[b]* and Audrey Moores[a]

**Abstract:** Amine *N*-alkylation is a process involved in the production of a wide range of chemicals. Here we describe the synthesis of well-defined (Ni$_{0.5}$Cu$_{0.5}$)Fe$_2$O$_4$ magnetic nanoparticles by plasma induction, and their successful application to amine *N*-alkylation using alcohols as coupling agents through a borrowing hydrogen pathway. Plasma induction allows precise morphology and size control over nanoparticle synthesis, while allowing the one-pot production of decagram quantities of material. Up to date, such nanoparticles have never been applied for organic reactions. By coupling high-end characterization techniques with catalytic optimization, we showed that small Cu(0) satellite nanoparticles played an essential role in alcohol oxidation, whereas both Ni and Cu were required for the last step of the reaction. Using elemental mapping, we demonstrated that catalyst deactivation occurred through a leaching/re-deposition mechanism of Cu and Ni onto the small Cu(0) nanoparticles. The reactions were conducted under microwave conditions, which exerted a positive effect on catalytic activity. Finally, the catalyst was active at low metal loadings (2 mol%) even on the gram-scale, and affording unprecedented TON for Ni/Cu bimetallic systems (19).
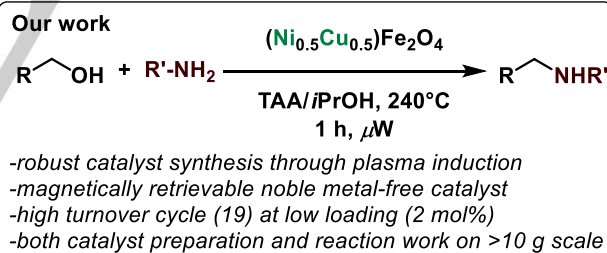
## Introduction

Amines are essential synthetic building blocks for the chemical industry and for numerous biological processes.[1] Synthetic amines are widely employed in pesticides, pharmaceuticals, dyes, detergents, polymers, lubricants and various other functional materials.[2] For their synthesis, a wide variety of processes is available, such as using halides or tosylates as alkylating agents through the Buchwald-Hartwig coupling. However, these coupling partners are toxic, and generate stoichiometric amounts of salts as byproduct. Alternatively, alcohols can be used as safer alkylating agents, generating only H$_2$O as a byproduct (Scheme 1Scheme 1).[3] They can be activated for C-N coupling *via* their *in situ* dehydrogenation towards the corresponding carbonyl, which enables offsetting their lower electrophilic reactivity. They can then condense with the amine, forming an imine and water as the

sole byproduct. The hydrogens "borrowed" from the alcohol can then be re-used to reduce the C=N bond, therefore affording the amine. Overall, the process is redox-neutral, and is referred to as 'borrowing hydrogen' (BH). Since the early works of Watanabe[4] and Grigg[5] with Ru and Ir complexes as catalysts, inspired by Crabtree's alcohol dehydrogenation chemistry[6] [7] and through the seminal works of Fujita[8] and Williams,[9] homogeneous BH has largely evolved from expensive metals and ligands, to base metals.[10] Although most reports are still based on Ru[11] and Ir, recent efforts have focused on base metals such as Fe,[12] [13] [14] Mn[15] and Co.[16] [17] {Rösler, 2015 #68}[16][16]



**Alcohol amination *via* borrowing hydrogen**
-one-pot and reductant-free
-H$_2$O as sole byproduct
-redox neutral process
-safe coupling agents

| Homogeneous catalysts | Heterogeneous catalysts |
|---|---|
| **Ru, Ir, Fe, Co, Mn** | **Ru, Ag, Fe, Cu, Ni** |
| -more active and selective | -harsher conditions |
| -non-recyclable | -recyclable |
| -expensive ligands | -non-scalable synthesis |

**Our work**

$$R\text{—}OH + R'\text{-}NH_2 \xrightarrow[\text{1 h, }\mu W]{\substack{(Ni_{0.5}Cu_{0.5})Fe_2O_4 \\ TAA/iPrOH, 240°C}} R\text{—}NHR'$$

-robust catalyst synthesis through plasma induction
-magnetically retrievable noble metal-free catalyst
-high turnover cycle (19) at low loading (2 mol%)
-both catalyst preparation and reaction work on >10 g scale

**Scheme 1:** Overview of alcohol amination through BH pathway.

In an effort to overcome recycling and separation issues associated with these expensive metal complexes, heterogeneous catalysts were extensively explored.[18] Both Ru NPs supported on Fe$_3$O$_4$[19] and Ag NPs have shown a strong potential.[20] [21] [22][20] From our perspective though, abundant metals should be favored to exploit the full potential of heterogeneous catalysis towards eco-friendlier processes.

To palliate this issue, some authors have adopted bBimetallic catalysts have proven particularly attractive, enabling synergistic effects (Au-Pd),[23] and also allowing "dilution" of the precious metal with a cheaper one (Ag-Cu,[20] Pt-Sn,[24] Cu-Al[23], Cu-Au[25], Pd-Zn[26], Co-Rh[27]). SFrom our perspective though, abundant
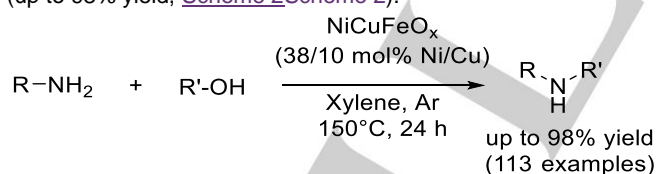
[a] A.Y. Li, A. Segalla, Prof. A.H. Moores
Centre for Green Chemistry and Catalysis
McGill University
801 Sherbrooke street West, Montreal, QC H3A 0B8
E-mail: Audrey.Moores@mcgill.ca
[b] N. Dumaresq, Prof. N. Braidy
Département de génie chimique et de génie biotechnologique
University of Sherbrooke
2500, boul. de l'Université Sherbrooke, Sherbrooke, QC J1K 2R1
E-mail : Nadi.Braidy@usherbrooke.ca

Supporting information for this article is given via a link at the end of the document.
† Alain Li and Nicolas Dumaresq have contributed equally to this article

metals should be favored to exploit the full potential of heterogeneous catalysis towards eco-friendlier processes. Some others have explored [I would move here the line on bimetallic, and list all the ones with at least one precsous metals]. From our perspective though, abundant metals should be favored to exploit the full potential of heterogeneous catalysis towards eco-friendlier processes. $Fe_3O_4$ NPs,[28] Cu NPs,[29] zeolites,[30] Cu-Al[31], and even metal-free graphene oxide sheets[32] have been reported as catalysts for alcohol amination. In most examples though, a base (KOH, $K_2CO_3$) is required to promote the proton removal in the alcohol oxidation step. Yet, the presence of a base is undesirable during the reaction as it may also favor side reactions typical for alcohols and transient carbonyls (Cannizzaro condensation, alcohol dehydration, and aldol condensation). Notably, hHeterogeneous Ni has been widely explored since its first report in 1932 by Winans et al., requiring though 100 bar $H_2$ at 200°C for the alkylation of cyclohexylamine with EtOH.[33] Ni has also been shown by Shimizu and others to be highly competent for BH when supported on $\theta$-$Al_2O_3$,[34] and can even perform ammonia alkylation in flow synthesis.[35]-[36] In most examples though, a base (KOH, $K_2CO_3$) is required to promote the proton removal in the alcohol oxidation step. Yet, the presence of a base is undesirable during the reaction as it may also favor side reactions typical for alcohols and transient carbonyls (Cannizzaro condensation, alcohol dehydration, and aldol condensation). However, Ni is a carcinogenic and allergenic metal, driving the search towards partial substitution with other metals, for instance Cu.[37] In order to circumvent this issue, other authors have adopted bimetallic catalysts (Au-Pd,[28] Ag-Cu,[29] Pt-Sn,[30] Cu-Al[31], Cu-Au[32], Pd-Zn[33], Co-Rh[34]). The most notable example is the Ni/Cu pair forThe Ni/Cu pair is alsoindeed active for alcohol amination: Cu acts as a dehydrogenation catalyst for the starting alcohol, while Ni performs the hydrogenation of the imine.[38] Cu and Ni stearates with various stabilizers such as Ba stearate have been reported the production of long alkyl chains N,N-dimethylamines.[39] The Shi group reported a $NiCuFeO_x$ catalyst (3.6/1.1/1 weight ratio) through the calcination of metal carbonates then reduction under a $H_2$ flow.[40] Their alcohol amination scope was extensive, with 113 examples (up to 98% yield, Scheme 2Scheme 2).

$$R-NH_2 \quad + \quad R'\text{-}OH \xrightarrow[\substack{\text{Xylene, Ar} \\ 150°C,\ 24\ h}]{\substack{NiCuFeO_x \\ (38/10\ \text{mol\%}\ Ni/Cu)}} \underset{H}{R\text{-}\overset{R'}{N}}$$

up to 98% yield
(113 examples)

**Scheme 2**. Former example of Ni/Cu for alcohol amination.

In all these examples, NP synthesis are produced using well-established synthesis methods such as coprecipitation or sol-gel. These methods are known for their good control on the particle size and composition. However, the synthesis steps can be time-consuming: in most cases, they can add up to 12 h and can suffer from batch-to-batch reproducibility issues. These drawbacks become problematic for a scaledd up of production to an industrial level for which the catalyst's properties need to be reproducible from one batch to the next. Additionally, in past reports,[39] Cu-Ni

ferrite catalysts characterization was limited to the identification of the major phases. However, more work is needed in order to pinpoint the active phase or and the relative role of Cu and Ni in the mechanism of the reaction, calling for an extensive characterization study detailing the nanostructure of the catalyst before and after reaction is needed.

Thus, developing waste-efficient synthesis of well-defined NPs on a big scale is imperative for far-reaching catalytic applications. Furthermore, despite their attractiveness, heterogeneous base metal catalysts (Cu, Ni, Mn, Fe) still require high loadings to offset their lower activity. For instance, up to 38 mol% Ni loading were required in Shi's report. A careful nanostructure design could minimize the metal amounts. To obtain crystalline and well-defined NPs, high temperatures are required to decompose NP precursor and allow ordered growth. In liquid phase though, ligand-free NP agglomeration is difficult to avoid, driving the search for solid-state[41] or gas phase processes.[42] Taking these considerations into account, we turned to induction plasma as a technique for the synthesis of Ni/Cu-containing NPs. Temperatures as high as ~6.000 K and ~10.000 K can be reached in plasma reaction chambers, allowing in situ annealing and precise phase control.[43] Through a strict control of precursor residence time and growth quenching, plasma induction allows the single-step production of monodisperse and crystalline NPs at high quantities (up to 30 g/h for 50 kW units) that is easily scalable with higher energy torches and larger reactors.[44] Radio-frequency (RF) plasma induction has already been used for the synthesis of ferric oxide nanoparticles from their corresponding metal nitrate salts, such as $ZnFe_2O_4$[45] and $NiFe_2O_4$.[46] To the best of our knowledge, no mixed ferrite synthesis from a RF plasma reactor has been reported so far. Herein we report the first example of nanocatalysts for alcohol amination, using $(Ni_{0.5}Cu_{0.5})Fe_2O_4$ NPs made by plasma induction. The catalyst was easily recyclable by magnetic separation and it was able to catalyze the reaction at low metal loadings comparable to that of homogeneous catalysts (<2 mol% of metal).

## Results and Discussion

First, $(Ni_{0.5}Cu_{0.5})Fe_2O_4$ NPs were synthesized in an induction thermal plasma reaction chamber, following a procedure already reported previously by us for the synthesis of $NiFeO_2$ NPs[46] and using a plasma setup described elsewhere (Figure 1Figure 1).[47] The synthesis consisted in the coaxial injection aqueous solution of metal precursors (Fe, Ni and Cu nitrates in a 4/1/1 molar ratio) with a carrier gas (Ar) into an inductively coupled thermal plasma torch. A sheath gas of $Ar/O_2$ was used to control the trajectory of the NPs and provide them with oxygen atoms. The tip of the atomization probe coincides with the center of an induction thermal plasma torch connected to a 3 MHz RF power supply. As shown in Figure 1Figure 1, the plasma torch connects into the top of a water-cooled cylindrical chamber (Main reactor).
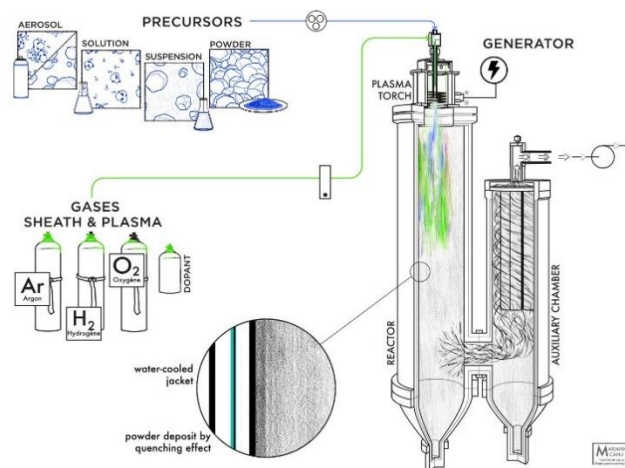
**Figure 1.** Schematic of inductively coupled radio-frequency plasma reaction chamber.

At its bottom, the main reactor is connected to another water-cooled cylindrical chamber (Auxiliary chamber) which contains 4 microporous filters connected to a vacuum pump. Upon evaporation of $H_2O$ as the carrier solvent of the precursors in the main chamber, homogeneous nucleation of nanoparticles occurs by precursor supersaturation in the plasma phase. The main reactor is designed to recirculate the NPs several times into the high temperature region (Figure 1, blue/green region). During this recirculation, the NPs undergo several melting, quenching and annealing cycles, favoring crystalline particle growth. The entrance of the auxiliary chamber is designed to generate a cyclone, through which only particles with a sufficient hydrodynamic size can pass through and deposit on the walls of the auxiliary chamber and the filters. With this apparatus, we investigated the synthesis of mixed Ni/Cu ferrite nanoparticles, using a 4/1/1 molar ratio of Fe/Cu/Ni in the precursor solution. We collected separately the resulting NPs from the main and the auxiliary chambers and called the resulting samples $(Ni_{0.5}Cu_{0.5})Fe_2O_4^{MAIN}$ and $(Ni_{0.5}Cu_{0.5})Fe_2O_4^{AUX}$ respectively. $(Ni_{0.5}Cu_{0.5})Fe_2O_4^{AUX}$ constituted about 33 wt% of the total powder collected. Both batches were subsequently tested for their catalytic activity.

**Characterization of fresh catalyst**

Catalyst bulk composition was analyzed by X-ray Fluorescence (Figure 2Figure 2). The metal ratios observed were close to the 4/1/1 molar ratios of injected precursors , similarly to our previous studies on the RF plasma synthesis of $NiFe_2O_4$.[46] In $(Ni_{0.5}Cu_{0.5})Fe_2O_4^{MAIN}$ a slightly higher amount of Cu (18.5 at% at compared to the expected value (16.7 at%% at) was observed, whereas a smaller amount of Cu was observed in $(Ni_{0.5}Cu_{0.5})Fe_2O_4^{AUX}$ (15.1 at%% at). The Ni amounts were consistently close to the expected value (16.7 at%) at 16.1 at% and 16.2 at% for $(Ni_{0.5}Cu_{0.5})Fe_2O_4^{MAIN}$ and $(Ni_{0.5}Cu_{0.5})Fe_2O_4^{AUX}$ respectively. Finally, the trend for Fe amounts was the opposite to that of the Cu amounts: 65.4 at% at and 68.8 at% at for $(Ni_{0.5}Cu_{0.5})Fe_2O_4^{MAIN}$ and $(Ni_{0.5}Cu_{0.5})Fe_2O_4^{AUX}$ respectively (66.7

at% at expected). These small discrepancies from the expected values could be explained by the boiling point of Cu (2540 K at 20 kPa, a pressure close to the one in the plasma reactor) that is lower compared to the one of Fe and Ni (2720 K and 2860 K at 20 kPa), causing Cu to remain longer into gas phase, condensate less and thus contribute less to the particles transferred to the auxiliary reactor.

Crystalline phase formed in the fresh catalyst was determined by using XRD. A Rietveld refinement of the diffractogram obtained confirm the sole presence of one crystalline $(Ni_xCu_y)Fe_{3-x-y}O_4$ spinel phase in both samples (Figure 3Figure 3 a-b). For $(NiCu_{0.5}CuNi_{0.5})Fe_2O_4^{AUX}$, these results are consistent with the XRF-obtained molar ratios. However, for $(CNiu_{0.5}NCui_{0.5})Fe_2O_4^{MAIN}$, the molar ratios no longer match, suggesting the presence of a separate Cu-rich phase. Such a phase has tomust be amorphous in nature or present as very small crystallites, since no second phase is was seen in observed byXRD.
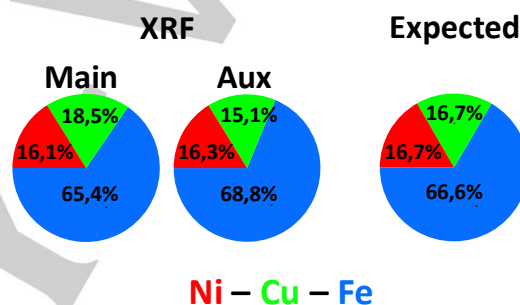


**Figure 2**: XRF analysis of the $(Ni_{0.5}Cu_{0.5})Fe_2O_4^{MAIN}$ and $(Ni_{0.5}Cu_{0.5})Fe_2O_4^{AUX}$.
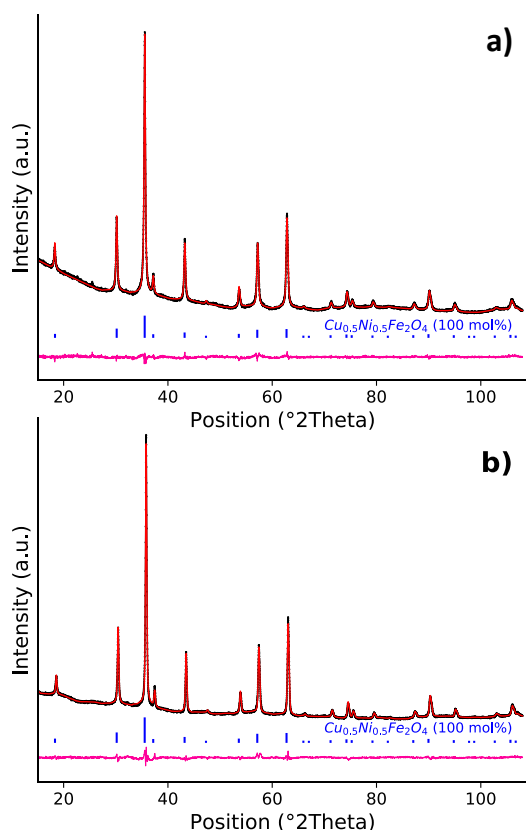
**Figure 3**: X-ray diffractogram of a) $(Ni_{0.5}Cu_{0.5})Fe_2O_4^{MAIN}$ b) $(Ni_{0.5}Cu_{0.5})Fe_2O_4^{AUx X}$ Experimental pattern (black line), calculated pattern by Rietveld refinement (red line) and the difference plot (purple line). The stick pattern are the references used for the Rietveld refinement.

To complete this analysis, an extensive study on $(Ni_{0.5}Cu_{0.5})Fe_2O_4^{MAIN}$ was performed trough transmission electron microscopy (TEM). The STEM-HAADF micrography of a representative region of interest of the sample $(Ni_{0.5}Cu_{0.5})Fe_2O_4^{MAIN}$ (Figure 4Figure 4a) shows an aggregate of nanoparticles that contain 3 different morphologies. The first are large (20-70 nm) faceted particles (truncated octahedrons shown in the yellow dash box), the second are irregular shaped agglomerates smaller than 5 nm (irregular yellow dash shape) and the last ones are smaller (2-4 nm) clusters decorating the other particles (white arrow). A magnified view of the region in the red box Figure 4Figure 4b) highlights a 2-3 nm cluster on which an intensity line profile is plotted in Figure 4Figure 4c and done and shows an average clusters size of 2-3 nm.

EELS elemental maps (Figure 4Figure 4d) were produced by integrating the background subtracted signal of the Cu (green), Ni (red) and Fe (blue) $L_{2,3}$ edges. The maps exhibit a uniform signal across the large faceted particles and the irregular shaped agglomerates indicating a uniform distribution in these structures. The O K edge map (not shown) correlates with the two Cu-Ni-Fe-rich structures which are consistent with the occurrence of (CuNi$_{0.5}$CuNi$_{0.5}$)Fe$_2$O$_4$ oxides identified by XRD (Figure 3Figure 3 a). However, the smaller clusters are rich in Cu, which is consistent with the brighter contrast observed in the STEM-HAADF

(Figure 4Figure 4a and b) characteristic of a higher average Z of metallic Cu compared to the oxides. Note that the EELS signal of the Cu-rich clusters that appears on the edge of the oxides is much stronger than the clusters that are superimposed to the large-faceted particles. This can be explained by the fact that the signal of the Cu-rich particle superimposed to the oxides is weakened by the scattering of a significant fraction of the electron beam by the larger particles. The signal-to-noise ratio of the smaller particles was too low to carry out EELS fingerprinting. To overcome this issue, we have turned to a multivariate analysis strategy. We begin by generating a trivariate histogram of the number of pixels having a given Cu, Ni and Fe relative intensities from the elemental EELS maps (Figure 5Figure 5a).The most prominent feature of the histogram has a Fe:Ni:Cu ratio of X:Y:Z and is related to the pixels composing the oxide phase. Knowing that two phases are present in the spectrum image, we selected two regions of interest on the histogram: one for the oxides, delimited by the green ellipse and the Cu-rich composition, delimited by the red triangle. The spectra of the pixels assigned to each region of interest were summed to create two reference spectra (Figure 5Figure 5 b-e): the first represents the sum of all the spectra of the oxide phase in the image (green curves) and the second corresponds to the joint spectrum of all pixels associated to the Cu-rich clusters (red curves).

The background preceding the O K edge of the spectrum image and the two reference spectra was then removed. We then used a linear least square routine to generate two fit-coefficient maps (Figure 5Figure 5 f) that shows the spatial distribution of the two reference spectra (oxides in green and Cu-rich phase in red). The large faceted particles and the irregular shaped agglomerates are consistent with our interpretation of the elemental maps[AM1] (Figure 4Figure 4 d). However, this multivariate analysis brings out better the smaller Cu-rich clusters (red), especially those that are not on the edge of the ferrites particles.[AM2] A significant difference is observed between the Cu $L_{2,3}$ EELS fingerprint of the two reference spectra (Figure 5Figure 5 e). The oxide spectrum (green) shows two distinct peaks at 931 eV and 950 eV corresponding to the white lines of Cu in the +2 oxidation state. However, the Cu-rich spectrum (red) does not show the white lines but exhibits a staircase-like profile located at 933 eV typical to the metallic state of a filled $d$ orbitals. This confirms the metallic nature of the Cu-rich particles. Note that metallic Cu was not identified in the XRD pattern of Figure 3Figure 3b. This is unsurprising because such a small content of 2-3 nm clusters does not significantly diffract X-rays to form detectable signal. The intensity of the Ni, Fe and O edges (Figure 5Figure 5 b-d) associated to the Cu-rich zones (red) are considerably weaker than the Cu edge signal when compared to the corresponding signals of the oxides. The O, Fe and Ni signal intensity decrease as the size of the integration region in the trivariate histogram tends towards the Cu end member, hence confirming the Cu-rich nature of the clusters. $(Ni_{0.5}Cu_{0.5})Fe_2O_4^{AUX}$ was analyzed as well with the same techniques (see Figure S1). In these samples, only the 20-70 nm truncated octahedron made of ferrite were observed. The 5 nm ferrite agglomerates and 2-3 nm Cu NPs were absent.
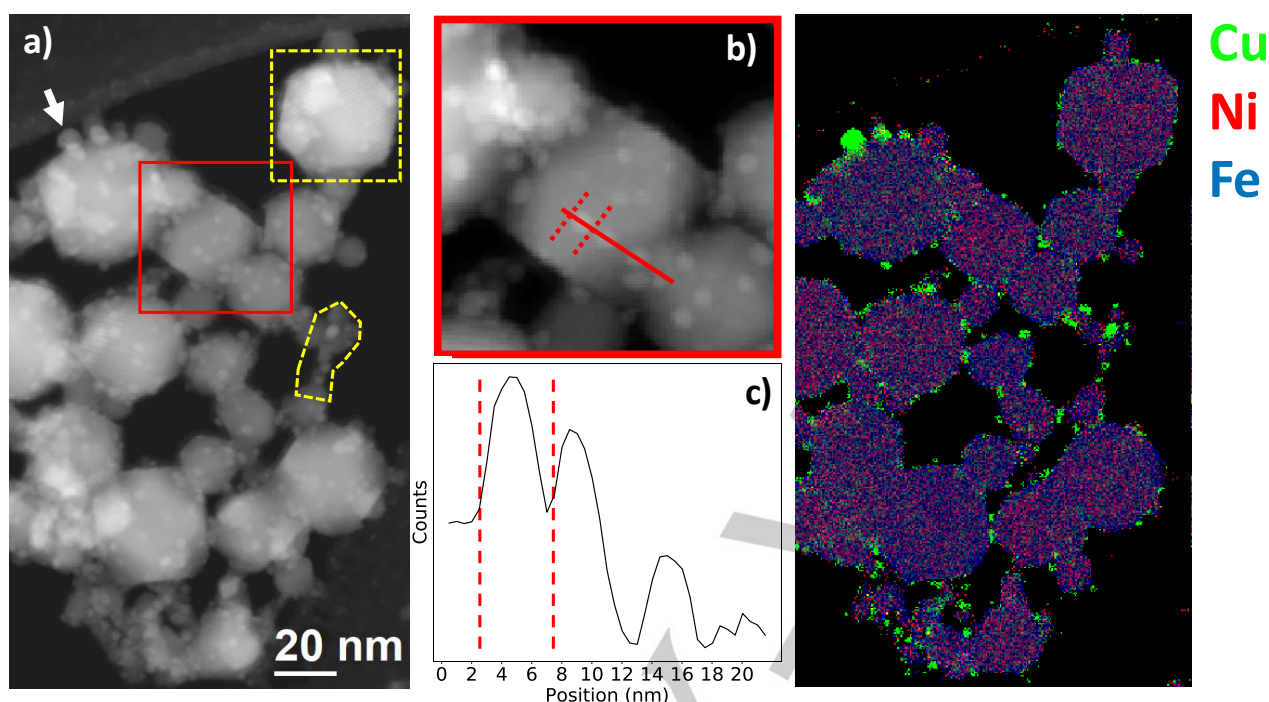
**Figure 4:** a) STEM-HAADF micrograph of a representative region of fresh $(Ni_{0.5}Cu_{0.5})Fe_2O_4^{MAIN}$. b) Details of a region of interest of the STEM-HAADF of $(Ni_{0.5}Cu_{0.5})Fe_2O_4^{MAIN}$. c) Intensity profile from Cu clusters decorating the oxide phase. d) EELS elemental map of Cu (green), Ni (red), Fe (blue) of the STEM-HAADF map shown in a).
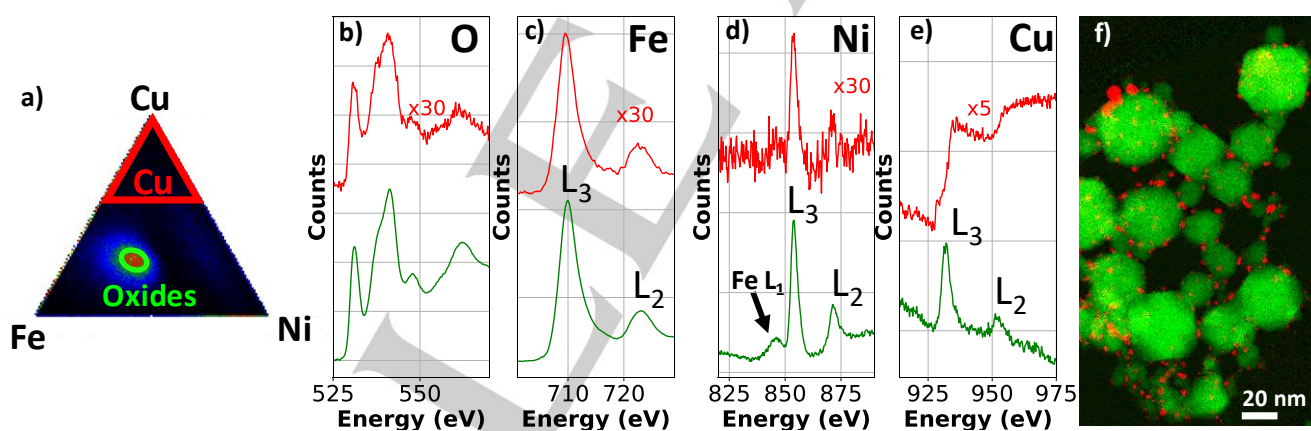


**Figure 5:** a) Trivariate histogram made with the background-subtracted metal edges computed for each pixels of the EELS spectrum images of the fresh $(NiCu_{0.5}CuNi_{0.5})Fe_2O_4^{MAIN}$. EELS edges of b) O K c) Fe $L_{2,3}$ d) Ni $L_{2,3}$ e) Cu $L_{2,3}$ of the reference spectra of the phases marked in the trivariate histogram: oxides phase (blue) and the Cu-rich phase (green) and the Cu-Ni rich phase (red) f) Fit-coefficient maps of the reference spectra of the oxides (green), Cu-rich (red) phases.

The oxide composition determined form the reference spectra (**Error! Reference source not found.**Table 1) closely corresponds to the initial ratio injected into the plasma reactor, in agreement with XRD analysis. The Cu-rich clusters account for the difference in the Cu content of the oxide particles deduced by EELS and the Cu fraction of the precursors. The presence of the Cu clusters is consistent with the XRF bulk analysis that confirms the higher Cu content of the sample collected in the main reactor. XPS analysis was performed as well to determine the surface composition, and a full discussion is provided in supporting information (Table S2).

**Table 11:** ~~Oxide~~ Elemental composition of the truncated octahedron oxide NPs in $(Ni_{0.5}Cu_{0.5})Fe_2O_4^{MAIN}$ calculated from the EELS reference spectrum, ~~as compared to the composition of what is injected in the reactor.~~

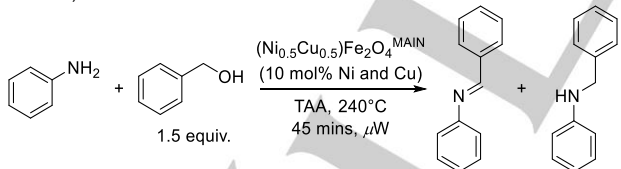| Sample | ~~EELS [AM3]E~~elementals content | | | |
|---|---|---|---|---|
| | Cu | Ni | Fe | O |
| Oxide (truncated octahedrons in $(Ni_{0.5}Cu_{0.5})Fe_2O_4^{MAIN}$) | 0.058 | 0.089 | 0.306 | 0.545 |
| ~~Perfect spinel from injected~~Injected in the reactor | 0.071 | 0.071 | 0.286 | 0.571[a] |

[a] Oxygen content calculated assuming a perfect ~~the~~ spinel stoichiometry

## Catalytic results

We first tested $(Ni_{0.5}Cu_{0.5})Fe_2O_4^{MAIN}$ for the base-free condensation of aniline with benzyl alcohol (Table 2Table 2**Error! Reference source not found.**). In order to ensure a higher reaction reproducibility and pressure control, we opted for microwave heating. Thus, we chose *tert*-amyl alcohol (TAA) as a solvent due to its compatibility with microwave heating and its absence of α-H relative to its hydroxy group, making it inert towards dehydrogenation. Under the conditions described below, reaction pressure reached up to 26 bar. A typical temperature and pressure profile is provided in the supporting information (Chart S1 and S2). Using one equivalent of benzyl alcohol with the aniline and 10 mol% of the catalyst, we initially obtained 15% of the desired amine along with 64% of the imine after 45 minutes of microwave heating at 240°C (Table 2Table 2**Error! Reference source not found.**, entry 1). We reasoned that addition of an excess of reducer, which in this case is the substrate benzyl alcohol, could push the desired hydrogenation of imine. This indeed increased the yield to 51 and 56%, for respectively 1.5 and 2 equivalents of alcohol (Table 2Table 2**Error! Reference source not found.**, entries 2 and 3). Thus, we kept the alcohol excess to 1.5 for the rest of**Error! Reference source not found.** experiments. Diminishing the catalyst amount from 50 mg to 40 mg decreased the yield from 51% amine and 36% imine to 29% amine and 60% imine (Table 2Table 2**Error! Reference source not found.**, entry 4), but increasing the catalyst amount to 60 mg decreased the yield as well to 27% amine and 50% imine (Table 2Table 2**Error! Reference source not found.**, entry 5). The imine product formation was above 26% in entries 1-5, hinting at the difficulty of the catalyst to perform C=N reduction. As we did not want to push beyond adding 1.5 excess of benzyl alcohol, we turned to adding 10 vol% of *i*PrOH, a classic sacrificial hydrogen donor, to our solvent system, increasing the yield to 78% (Table 2Table 2**Error! Reference source not found.**, entry 6).
.

**Table 2:** Reaction of aniline with benzyl alcohol in the presence of $(Ni_{0.5}Cu_{0.5})Fe_2O_4^{MAIN}$ under various conditions.[a]



| Entry | Modification | | Yield (%) | |
|---|---|---|---|---|
| | | | Imine | Amine |
| 1 | Benzyl alcohol excess | 1 | 64 | 15 |
| 2 | | 1.5 | 36 | 51 |
| 3 | | 2 | 26 | 56 |
| 4 | Catalyst quantity | 40 mg[b] | 60 | 29 |
| 5 | | 60 mg[c] | 50 | 27 |
| 6 | *i*PrOH additive (10 vol%) | | 2 | 78 |

[a] Standard reaction conditions: aniline (1 mmol), benzyl alcohol (1.5 mmol), $(Ni_{0.5}Cu_{0.5})Fe_2O_4^{MAIN}$ (50 mg, 10 mol% of Ni and 10 mol% Cu), *tert*-amyl alcohol (2 mL), Ar, microwave, 240°C, 45 min. [b] 8 mol% of Ni and Cu [c] 12 mol% of Ni and Cu

Since the addition of 10 vol% *i*PrOH proved fruitful to assist C=N reduction, we could lower the excess of benzyl alcohol to 1.2

equivalents and pushed the yield to above 70% while minimizing the imine amount to <2% (Table 3Table 3). Such an alcohol excess is commonly encountered for catalytic systems in this field, even in homogeneous catalysis.[48] With this system we studied the reaction kinetics to better understand the catalytic system and optimize the reaction time, which was fixed to 45 min in all runs described so far. As the reaction proceeds, benzyl alcohol is first consumed rapidly, and is almost completely gone after 30 minutes of reaction (Table 3Table 3**Error! Reference source not found.**, entry 4). As could be expected, the imine rapidly builds up as the alcohol gets dehydrogenated and reaches a maximum at 10 min, before slowly dropping, as the amine is steadily produced. Past 55 min of reaction, a plateau of 72-77% yield was reached for the amine with virtually no imine left (<2%) (Table 3Table 3**Error! Reference source not found.**, entries 5-8). Between 75 and 90 min, the amine gets re-oxidized back into the imine (41 and 32% respectively) (Table 3Table 3**Error! Reference source not found.**, entry 9). With these results in hand, we settled at 1 h for the optimum reaction time.

**Table 3**: Time optimization of the model reaction using *i*PrOH as an additive.[a]
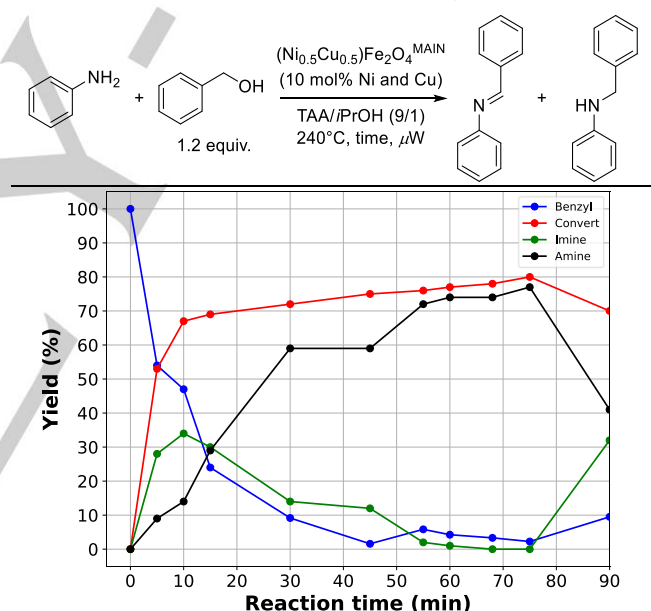


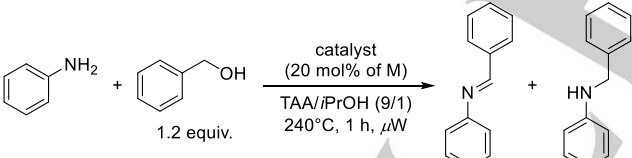| Entry | Reaction time | Yield (%) | |
|---|---|---|---|
| | | Imine | Amine |
| 1 | 5 | 28 | 9 |
| 2 | 15 | 30 | 29 |
| 3 | 30 | 14 | 59 |
| 4 | 45 | 12 | 59 |
| 5 | 55 | 2 | 72 |
| 6 | 60 | 1 | 74 |
| 7 | 68 | <1 | 74 |
| 8 | 75 | <1 | 77 |
| 9 | 90 | 32 | 41 |

[a] Standard reaction conditions: aniline (1 mmol), benzyl alcohol (1.2 mmol), $(Ni_{0.5}Cu_{0.5})Fe_2O_4^{MAIN}$ (50 mg, 10 mol% of Ni and 10 mol% Cu), *tert*-amyl alcohol/isopropanol (1.8 mL and 0.2 mL), Ar, microwave, 240°C.

## Mechanistic study: insight into the catalytic site

We tested different ferrite-based catalysts using our plasma induction method, in order to probe the role of each metal. Using metal ferrites from the main reactor composed of only one of the

two catalytic metals tested, namely $CuFe_2O_4^{MAIN}$ or $NiFe_2O_4^{MAIN}$, drastically decreased the yield to 5% and 1% in amine respectively, with an imine yield of 10% and 4% respectively (Table 4Table 4Error! Reference source not found., entries 2 and 3). Mixing in the same batch independently prepared $CuFe_2O_4^{MAIN}$ and $NiFe_2O_4^{MAIN}$ NPs yielded 37% of amine and 36% of imine, confirming that both Cu and Ni are required for the reaction (Table 4Table 4Error! Reference source not found., entry 4). Importantly having Cu and Ni within the same particle seems to help with imine reduction to amine, as the comparable run with $(Ni_{0.5}Cu_{0.5})Fe_2O_4^{MAIN}$ provided 74% in amine and 1% in imine (Table 4Table 4Error! Reference source not found., entry 1). Using $Fe_3O_4^{MAIN}$ NPs gave no product (Table 4Table 4Error! Reference source not found., entry 5). Also, up to now we had focused on studying $(Ni_{0.5}Cu_{0.5})Fe_2O_4^{MAIN}$ from the main reactor. We also wanted to test $(Ni_{0.5}Cu_{0.5})Fe_2O_4^{AUX}$ collected on from the filter of the auxiliary reactors. These afforded much lower yields (8% amine yield with 18% imine, Table 4Table 4 entry 6). Since the main compositional difference between $(Ni_{0.5}Cu_{0.5})Fe_2O_4^{AUX}$ and $(Ni_{0.5}Cu_{0.5})Fe_2O_4^{MAIN}$ resides in the absence of small Cu(0) satellite NPs in the former, we can infer from this result that these species play a key role in the amine alkylation reaction. Finally, using either $CuFe_2O_4^{AUX}$ or $NiFe_2O_4^{AUX}$ from the filter gave similar trends to the ones with $CuFe_2O_4^{MAIN}$ and $NiFe_2O_4^{MAIN}$ (8 and 1% yield with 6 % and 2% imine, Table 4Table 4 entries 7 and 8), although with lower yields. It is worth noting that in almost every case involving only Ni or Cu (Table 4Table 4Error! Reference source not found., entries 2, 3, 7 and 8), the mass balance for N-containing products dropped below 75%, whereas it remained higher than 90% when both metals were present (Table 4Table 4Error! Reference source not found., entries 1, 4 and 6). This mass balance issue is further discussed in the supporting information.

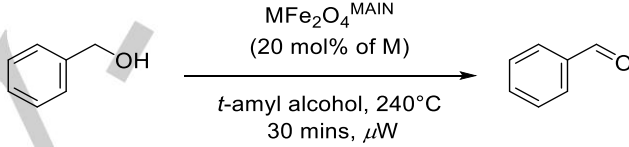**Table 4:** Control experiments.[a]



| Entry | | Modification | Conversion | Yield (%) | |
|---|---|---|---|---|---|
| | | | | Imine | Amine |
| 1 | Catalyst$^{MAIN}$ | $(Ni_{0.5}Cu_{0.5})Fe_2O_4^{MAIN}$ | 77 | 1 | 74 |
| 2[b] | | $CuFe_2O_4^{MAIN}$ | 33 | 10 | 5 |
| 3[c] | | $NiFe_2O_4^{MAIN}$ | 30 | 4 | 1 |
| 4[d] | | $CuFe_2O_4^{MAIN}$ and $NiFe_2O_4^{MAIN}$ | 79 | 36 | 37 |
| 5 | | $Fe_3O_4^{MAIN}$ | 22 | 3 | 0 |
| 6[d] | Catalyst$^{AUX}$ | $(Ni_{0.5}Cu_{0.5})Fe_2O_4^{AUX}$ | 34 | 18 | 8 |
| 7[b] | | $CuFe_2O_4^{AUX}$ | 52 | 6 | 8 |
| 8[c] | | $NiFe_2O_4^{AUX}$ | 40 | 2 | 1 |

[a] Standard reaction conditions: aniline (1 mmol), benzyl alcohol (1.2 mmol), catalyst (50 mg), *tert*-amyl alcohol/isopropanol (1.8/0.2 mL), Ar, microwave, 240°C, 1h [b] 20 mol% Cu [c] 20 mol% Ni [d] 10 mol% Ni and 10 mol% Cu

Then, we looked at the role of each metal in the mechanistic pathway. To better probe the alcohol dehydrogenation step, we heated benzyl alcohol alone under microwave conditions in the presence of various catalysts under inert conditions (240°C, 1h). With $(Ni_{0.5}Cu_{0.5})Fe_2O_4^{MAIN}$, 97% of the benzyl alcohol got consumed into various oxidations products: benzaldehyde, benzoic acid, and benzyl benzoate (Table 5Table 5Error! Reference source not found., entry 1). Under inert atmosphere, the presence of benzaldehyde can only be explained through a dehydrogenation pathway. Subsequently, benzaldehyde can undergo Cannizzaro dismutation at elevated temperature to form benzoic acid.[49] Finally, the last product can condense with benzyl alcohol to form benzyl benzoate. Upon using $CuFe_2O_4^{MAIN}$, a similar conversion of 84% was observed (Table 5Table 5Error! Reference source not found., entry 2). However, $NiFe_2O_4^{MAIN}$ alone gave a 25% conversion (Table 5Table 5Error! Reference source not found., entry 3).

**Table 5:** Mechanistic investigation on $(Ni_{0.5}Cu_{0.5})Fe_2O_4^{MAIN}$-catalyzed alcohol dehydrogenation.[a]
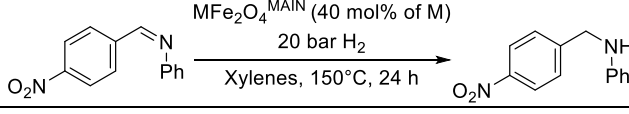


| Entry | Catalyst | Conversion (%) |
|---|---|---|
| 1 | $(Ni_{0.5}Cu_{0.5})Fe_2O_4^{MAIN}$ | 97 |
| 2[b] | $CuFe_2O_4^{MAIN}$ | 84 |
| 3[c] | $NiFe_2O_4^{MAIN}$ | 25 |

[a] Standard reaction conditions: benzyl alcohol (1 mmol), $(Ni_{0.5}Cu_{0.5})Fe_2O_4^{MAIN}$ (50 mg, 10 mol% of Ni and 10 mol% Cu), *t*-amyl alcohol (2 mL), Ar, microwave, 240°C, 30 min. [b] 20 mol% Cu [c] 20 mol% Ni

Finally, we investigated the last step of the mechanism, imine reduction. We first made an imine model substrate by ball-milling the corresponding aldehyde and amine in presence of a drying agent ($Na_2SO_4$) for 15 minutes. Then, we then subjected the imine to hydrogenation conditions (150 °C, 20 bar $H_2$) in presence of $MFe_2O_4^{MAIN}$ (M = Cu, Ni, $Ni_{0.5}Cu_{0.5}$) for 24 h. With $(Ni_{0.5}Cu_{0.5})Fe_2O_4^{MAIN}$, 30% of the imine was reduced into the corresponding amine (Table 6Table 6Error! Reference source not found., entry 1). In contrast, switching to $CuFe_2O_4^{MAIN}$ or $NiFe_2O_4^{MAIN}$ gave lower to no yield (0 and 5% respectively, Table 6Table 6Error! Reference source not found., entries 2 and 3). Such contrast in the catalytic results reveal that both Cu and Ni are needed, on the same nanoparticle and that they act in synergy in the hydrogenation of C=N bonds.

**Table 6:** Mechanistic investigation on $(Ni_{0.5}Cu_{0.5})Fe_2O_4^{MAIN}$-catalyzed imine reduction.[a]



| Entry | Catalyst | Yield (%) |
|---|---|---|
| 1 | $(Ni_{0.5}Cu_{0.5})Fe_2O_4^{MAIN}$ | 30 |

| | | |
|---|---|---|
| 2[b] | $CuFe_2O_4^{MAIN}$ | 0 |
| 3[c] | $NiFe_2O_4^{MAIN}$ | 5 |

[a] Standard reaction conditions: imine (0.5 mmol), $(Ni_{0.5}Cu_{0.5})Fe_2O_4^{MAIN}$ (50 mg, 20 mol% of Ni and 20 mol% Cu), Xylenes (15 mL), $H_2$ (20 bar), 150°C, 24 h. [b] 40 mol% Cu [c] 40 mol% Ni

Overall, our best catalyst was $(Ni_{0.5}Cu_{0.5})Fe_2O_4^{MAIN}$ (1% imine, 74% amine). Our test where Cu and Ni are separated, in the $CuFe_2O_4^{MAIN}$ and $NiFe_2O_4^{MAIN}$ mixture, led to a decrease of the amine yield but did not affect overall conversion (36% imine, 37% amine). However, using $(Ni_{0.5}Cu_{0.5})Fe_2O_4^{AUX}$ gave only 18% imine, 8% amine yield. The main different difference between $(Ni_{0.5}Cu_{0.5})Fe_2O_4^{AUX}$ and $(Ni_{0.5}Cu_{0.5})Fe_2O_4^{MAIN}$ being nanoparticles produced in the main reactor, vs the auxiliary reaction is the presence of small Cu(0) NPs on the latter, we can infer that these satellite NPs are responsible for alcohol dehydrogenation under our conditions. of the amorphous small clusters of metal zero Cu in the former. This suggests that these small Cu cluster are uniquely able to oxidize the alcohol under our conditions. The second step of the mechanism consists in the condensation of the resulting carbonyl with the amine to form an imine after the loss of a water molecule. Although the elevated temperature in our reaction favors $H_2O$ elimination, we cannot exclude metal cations in the spinel lattice acting as Lewis acid to help condensation to the imine.[50] Due to $CuFe_2O_4^{MAIN}$ being unable to perform the full process despite being able to dehydrogenate the oxidize alcohol, we can then deduce that a Ni species (identified by EELS to be Ni integrated to the ferrite lattice) performs the C=N reduction step. Furthermore, the presence of both Cu and Ni within the same nanostructure is required in order to further push imine reduction to completion, probably facilitating hydrogen transfer between the two metals. This is further supported by the tests performed in Table 6 Table 6, showing that Cu and Ni were both required for imine hydrogenation. Overall, such role assignment for Cu and Ni in alcohol amination is consistent with previous literature studies (Scheme 3 Scheme 3).[38] Finally, ICP-MS measurement on the organic mixture revealed the presence of respectively 0.18 ppm of Cu, 0.02 ppm of Fe, and 0.02 ppm of Ni after 18 turnover cycles. There is thus a very limited leaching into the end product, which is an important feature of commercial catalysts. To put in perspective, the permitted concentrations of residual metals in drugs in ICH Q3D (based on a maximum oral dose of ≤10 g per day) are as follows: 20 ppm for Ni and 300 ppm for Cu.[51] This confirms a purely heterogeneous mechanism for this reaction.
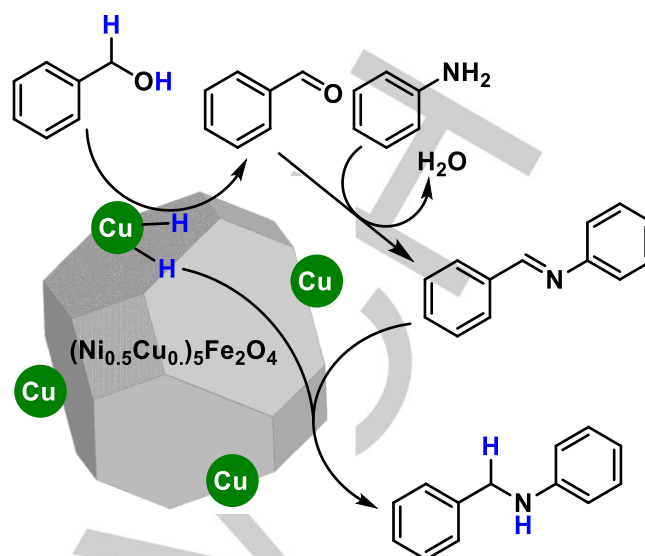


**Scheme 3.** Proposed mechanistic pathway for $(Ni_{0.5}Cu_{0.5})Fe_2O_4^{MAIN}$-catalyzed alcohol amination.

### Mechanistic studies: role of microwave heating

We then investigated the effect of microwave on the catalyst. All tests described until now were performed in standard glass vials, which are transparent to microwaves. Heating occurs then through the interaction of microwaves with matter inside the vials. Conversely, silicon carbide (SiC) vials are able to fully absorb microwave irradiations themselves, so that they can heat and shelter the material inside the vial from any radiation.[52] Using SiC vials, we could then test our catalysis under the same conditions of temperature and pressure, while providing purely thermal heating to the solution. Upon using a SiC vial, the yield in amine decreased from 74% to 30% (Table 7**Error! Reference source not found.**, entries 1 and 2). We also wanted to compare with a pure thermal setup, yet we had to slightly modify the conditions as we could not reproduce our optimal setting thermally. Since the model reaction reached up to 26 bar under microwave at 240°C, we ran it at lower temperature (130°C, 48h) to run it at oil bath conditions (Table 7**Error! Reference source not found.**, entries 3 and 4). Under these settings, a 11% yield was obtained under microwave heating whereas 5% of yield was obtained when the reaction was conducted in the oil bath. This combination of results clearly indicates that microwave conditions are highly beneficial in our $(Ni_{0.5}Cu_{0.5})Fe_2O_4^{MAIN}$-catalyzed reaction, with a 2/2.5-fold yield increase compared to convective heating conditions. Such activity boost under microwave has been observed previously on other magnetic nanocatalysts, such as $CrO_2$ for arene oxidation.[53] This could be attributed to local superheating phenomenon around the catalyst,[54] consistently with previous studies on the behavior of $NiFe_2O_4$ under microwave.[55]

**Table 7:** Microwave control experiments on $(Ni_{0.5}Cu_{0.5})Fe_2O_4^{MAIN}$ [a]
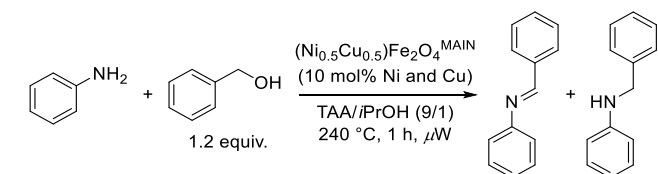
| Entry | Setup | Yield (%) | |
|---|---|---|---|
| | | Imine | Yield |
| 1 | Glass vial | 1 | 74 |
| 2 | SiC vial | 4 | 30 |
| 3 | Glass vial[b] | 2 | 11 |
| 4 | Glass vial, oil bath[b] | 1 | 5 |

[a] Standard reaction conditions: aniline (1 mmol), benzyl alcohol (1.2 mmol), $(Ni_{0.5}Cu_{0.5})Fe_2O_4{}^{MAIN}$ (50 mg), tert-amyl alcohol/isopropanol (1.8/0.2 mL), Ar, microwave, 240°C, 1h. [b] Same conditions at 130°C, 48h.

### Reaction scope

In order to understand the scope of the developed process, we tested the catalyst over a range of aniline derivatives (Table 7~~Ta-ble 8~~**Error! Reference source not found.**). 4-methylaniline, 4-nitroaniline and 4-methoxyaniline reacted in high yields with benzyl alcohol and gave respectively 71%, 67% and 68% yield (Table 7~~Table 8~~**Error! Reference source not found.**, entries 1-3). 4-chloroaniline, however, only afforded 21% yield (Table 7~~Table 8~~**Error! Reference source not found.**, entry 4) whereas 2-aminopyridine gave a 90% yield (Table 7~~Table 8~~**Error! Reference source not found.**, entry 5). In the case of benzamide only 15% yield was attained in the standard conditions, whereas 65% yield was afforded when *i*PrOH was removed (Table 7~~Table 8~~**Error! Reference source not found.**, entry 6), besides providing additional hydrogens to reduce the imine, is also a competitor for the alcohol dehydrogenation step. Thus, in this entry imine reduction occurs probably faster than in the model reaction, making the use of *i*PrOH detrimental to the reaction rate. However, benzenesulfonamide gave only 27% and 21% yield with or without *i*PrOH, respectively (Table 7~~Table 8~~**Error! Reference source not found.**, entry 7). Benzyl alcohol could also be successfully replaced with 2-methoxybenzyl alcohol, leading to a 75% yield (Table 7~~Table 8~~**Error! Reference source not found.**, entry 8).

**Table 8:** Reaction of benzyl alcohol with a range of aniline derivatives in the presence of $(Ni_{0.5}Cu_{0.5})Fe_2O_4{}^{MAIN}$



| Entry | Amine[a] | Product | Yield (%) |
|---|---|---|---|
| 1 | R=4-Me | | 71 |
| 2 | R=NO₂ ~~R=4-NO₂~~ | | 67 |
| 3 | R=OMe ~~R=4-OMe~~ | | 68 |
| 4 | R=4-Cl | | 21 |

| 5 | | | 90 |
| 6 | | | 15(65[b]) |
| 7 | | | 27(21[b]) |

| Entry | Alcohol[c] | Product | Yield (%) |
|---|---|---|---|
| 8 | | | 75 |

[a] Standard reaction conditions: amine (1 mmol), benzyl alcohol (1.2 mmol), $(Ni_{0.5}Cu_{0.5})Fe_2O_4{}^{MAIN}$ (50 mg, 10 mol% Cu and 10 mol% Ni), tert-amyl alcohol/isopropanol (1.8/0.2 mL), Ar, microwave, 240°C, 1h. [b] no isopropanol was used. [c] aniline (1 mmol), 2-methoxybenzyl alcohol (1.2 mmol), $(Ni_{0.5}Cu_{0.5})Fe_2O_4{}^{MAIN}$ (50 mg, 10 mol% Cu and 10 mol% Ni), tert-amyl alcohol/isopropanol (1.8/0.2 mL), Ar, microwave, 240°C, 1h.

Despite their high nucleophilicity, 1-hexylamine and piperidine gave no product, with a 0% starting amine recovery (Scheme 4~~Scheme 4~~). As for the sterically hindered diphenylamine, we have fully recovered the starting material with no conversion (Scheme 4~~Scheme 4~~).
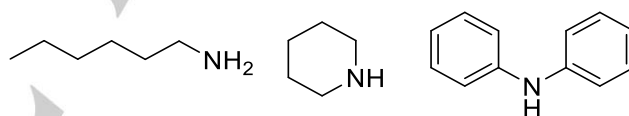


**Scheme 4.** Unsuccessful substrates.

We then turned to aliphatic short chain alcohols, used as both solvents and alkylating agents (Table 9~~Table 9~~**Error! Reference source not found.**). MeOH and EtOH remained inactive in our conditions (Table 9~~Table 9~~**Error! Reference source not found.**, entries 1 and 2). As for *n*-propanol, a 30/52 mixture of the mono- and di-alkylated amine was observed (Table 9~~Table 9~~**Error! Reference source not found.**, entry 3). Finally, for longer chains *n*-butanol and *n*-hexanol, 80 and 89% respectively of dialkylated product was observed, stemming from a higher stability of the aldehyde intermediates (Table 9~~Table 9~~**Error! Reference source not found.**, entries 4 and 5).

**Table 9.** Reaction of aniline with a range of aliphatic alcohols in the presence of $(Ni_{0.5}Cu_{0.5})Fe_2O_4{}^{MAIN}$ [a]



| Entry | Alcohol | Yield (%) | |
|---|---|---|---|
| | | Mono-alkyl | Bi-alkyl |
| 1 | MeOH[b] | 0 | 0 |
| 2 | EtOH[b] | 0 | 0 |
| 3 | *n*-propanol | 30 | 52 |

| | | | |
|---|---|---|---|
| 4 | *n*-butanol | 16 | 80 |
| 5 | *n*-hexanol | 11 | 89 |

[a] Standard reaction conditions: aniline (1 mmol), alcohol (2 mL), $(Ni_{0.5}Cu_{0.5})Fe_2O_4^{MAIN}$ (50 mg, 10 mol% of Ni and 10 mol% Cu), Ar, microwave, 200°C, 2h. [b] reactions were conducted at 165°C due to pressure constraints.

Empowered with a dialkylating catalyst, we decided to test a cyclizing reaction. Using 1,5-pentanediol as an electrophile, we successfully made in one-pot 1-phenylpiperidine through a double alkylation process (Scheme 5Scheme 5).
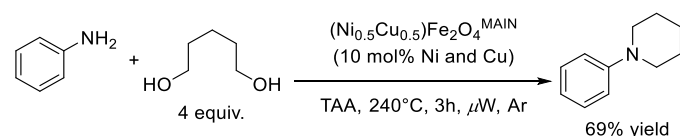


**Scheme 5.** Cyclization of 1,5-pentanediol with aniline catalyzed by $(Ni_{0.5}Cu_{0.5})Fe_2O_4^{MAIN}$.

We also tested $(Ni_{0.5}Cu_{0.5})Fe_2O_4^{MAIN}$ for the dehydrogenation of 1,2,3,4-tetrahydroquinoline under argon, as a test for the reverse of imine hydrogenation (Table 10Table 10). After 90 mins at 230°C, we observed the formation of 63% quinoline product (Table 10Table 10, entry 1). This indicates the ability of our catalyst to de-hydrogenate reactive C-N bonds, as well as C-C bonds in benzylic positions. Furthermore, this explains the yield decrease under prolonged conditions in our C-N coupling examples (see Table 3 **Error! Reference source not found.**). However, using only $CuFe_2O_4^{MAIN}$ or $NiFe_2O_4^{MAIN}$ reduced the yield to 17 and 2% respectively (Table 10Table 10, entries 2 and 3), hinting at both metals being necessary for amine dehydrogenation.

**Table 10.** Dehydrogenation of 1,2,3,4-tetrahydroquinoline.



| Entry | Catalyst | Yield (%) |
|---|---|---|
| 1 | $(Ni_{0.5}Cu_{0.5})Fe_2O_4^{MAIN}$ | 63 |
| 2[b] | $CuFe_2O_4^{MAIN}$ | 17 |
| 3[c] | $NiFe_2O_4^{MAIN}$ | 2 |

[a] Standard reaction conditions: 1,2,3,4-tetrahydroquinoline (1 mmol), $(Ni_{0.5}Cu_{0.5})Fe_2O_4^{MAIN}$ (50 mg, 10 mol% of Ni and 10 mol% Cu), *t*-amyl alcohol (2 mL), Ar, microwave, 230°C, 90 min. [b] 20 mol% Cu [c] 20 mol% Ni

**Recyclability and scale up**

Exploiting the magnetic properties of our ferrite-based catalyst, we could easily separate it from the reaction mixture using an external super-magnet. Upon washing it with acetone and drying in vacuum oven, we successfully re-used our catalyst 6 times with a 2-6% yield drop between each cycle (Table 11Table 11**Error! Reference source not found.**).

**Table 11.** Recycling experiments for $(Ni_{0.5}Cu_{0.5})Fe_2O_4^{MAIN}$-catalyzed condensation of aniline with benzyl alcohol.[a]



| Cycle | Imine (%) | Yield (%) |
|---|---|---|
| 1 | 1 | 74 |
| 2 | 2 | 68 |
| 3 | 5 | 64 |
| 4 | 7 | 62 |
| 5 | 8 | 58 |
| 6 | 10 | 56 |

[a] Standard reaction conditions: aniline (1 mmol), benzyl alcohol (1.2 mmol), $(Ni_{0.5}Cu_{0.5})Fe_2O_4^{MAIN}$ (50 mg), *tert*-amyl alcohol/isopropanol (1.8/0.2 mL), Ar, microwave, 240°C, 1h.

To test the applicability of $(Ni_{0.5}Cu_{0.5})Fe_2O_4^{MAIN}$, we scaled up the reaction to 8 mmol of aniline, obtaining a 66% yield (Table 12Table 12**Error! Reference source not found.**, entry 1). In these experiments we used a drastically reduced catalyst loading (1.9 mol% of Ni and Cu) and no TAA.[40] Subsequently, we scaled the model reaction further up to 32 mmol, with a similar yield of 62% (Table 12Table 12**Error! Reference source not found.**, entry 2).

**Table 12.** Reaction of aniline with benzyl alcohol in the presence of $(Ni_{0.5}Cu_{0.5})Fe_2O_4^{MAIN}$ on the gram scale.[a]



| Entry | Modification | Yield (%) | |
|---|---|---|---|
| | | Imine | Amine |
| 1 | - | 9 | 66 |
| 2 | 32 mmol scale [b] | 2 | 62 |

[a] Reaction conditions: aniline (8 mmol), benzyl alcohol (10 mmol), $(Ni_{0.5}Cu_{0.5})Fe_2O_4^{MAIN}$ (75 mg, 1.9 mol% of Ni and Cu), *i*PrOH(0.8 mL) Ar, microwave, 250°C, 90 min. [b] Previous amounts scaled to 32 mmol of aniline.

Based on both Cu and Ni amounts, our turnover number was 18 for Table 12, entry 1, and our cumulated turnover number was 19 after the 6 recycling cycles in Table 11. This value surpasses that of Shi's $NiCuFeO_x$ system reported earlier (11 TON, at 5.8 mol% Ni and 1.7 mol% Cu loadings).[40] Furthermore, it is worth noting that our catalyst proved to be active at low Cu/Ni loadings than theirs (1.9 mol% for each), comparable to that that of homogenous catalysts and without an additional base.
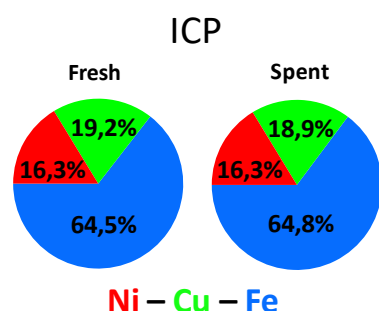
**Post-reaction characterization**

## ICP

**Fresh** **Spent**

Ni – Cu – Fe

**Figure 6**: ICP-MS $(Ni_{0.5}Cu_{0.5})Fe_2O_4{}^{MAIN}$ NPs before and after reaction : molar ratios of Ni, Cu and Fe.

Samples of $(Ni_{0.5}Cu_{0.5})Fe_2O_4{}^{MAIN}$ were subjected to 18 catalytic cycles. Their elemental analysis was done by ICP-MS after NPs digestion (Figure 6Figure 6), and the values were found to be very close, with a minor decrease in Cu content from 19.2 mol% to 18.9 mol%.

XRD followed by Rietveld refinement of the spent$(Ni_{0.5}Cu_{0.5})Fe_2O_4{}^{MAIN}$ (Figure 7Figure 7) confirmed that the spinel $Cu_{0.5}Ni_{0.5}Fe_2O_4$ structure was preserved during reaction. However, a second FCC phase of Cu(0) was also identified. ==The refinement showed a concentration of 77.5 wt%wt of spinel and 22.5 wt%wt of metallic copperCu(0). Note that the (002) peak of Cu(0) the metallic copper is abnormally large and will be discussed further on.==
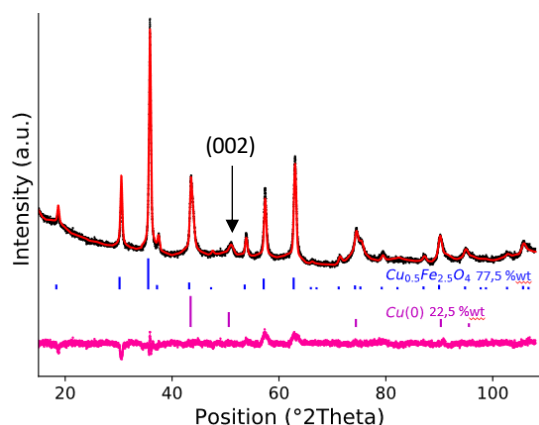


**Figure 7**: XRD pattern of $(Ni_{0.5}Cu_{0.5})Fe_2O_4{}^{MAIN}$ after 18 turnover cycles, Experimental pattern (black line), calculated pattern by Rietveld refinement (red line) and the difference plot (purple line). The stick pattern represents the reference pattern used for the Rietveld refinement.

STEM-HAADF micrographs of a representative region of the spent $Cu_{0.5}Ni_{0.5}Fe_2O_4{}^{MAIN\ air}$ catalyst after 20 turnover cycles are provided in Figure 8Figure 8 aError! Reference source not found.). Two distinct morphologies were observed on spent catalysts: (i) large facetted NPs as darker particles (as seen in red box) and (ii) large, irregular shaped particles with brighter contrast (example marked by red arrow). Compared to unspent fresh catalysts (Figure 5Figure 5a), we note that irregular shaped agglomerates and the clusters were not found in the spent catalyst, while the a new phase (ii) emergedappeared. Large facetted NPs (i) featured a new, porous-like texture (red box) likely due to a chemical degradation.
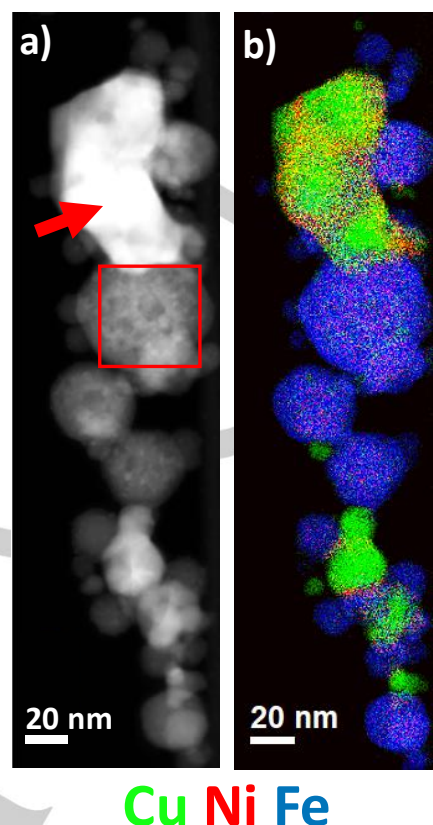


Cu Ni Fe

Figure 8: a) STEM-HAADF map of a representative region of the spent $(Ni_{0.5}Cu_{0.5})Fe_2O_4{}^{MAIN}$. b) EELS elemental map of Cu (Red), Ni (Green), Fe (Blue) of the STEM-HAADF map shown in a)

EELS elemental maps were produced in the same way as for fresh catalysts, by integrating the background subtracted signal of the Cu (red), Ni (green) and Fe (blue) $L_{2,3}$ edges (**Error! Reference source not found.**Figure 8b). he EELS maps of the large facetted NPs show a uniform chemical distribution. As it was the case with the facetted NPs of the fresh catalyst, no chemical segregation was apparent in these particles. The chemical composition O:(Fe,Ni,Cu) atomic ratio computed using the elemental EELS maps] of the large facetted particles corresponds to the (Ni,CuCu,Ni)$Fe_2O_4$ oxides identified by XRD (Figure 7Figure 7). The elemental EELS maps of the bright regions revealed the presence of a non-uniform (Ni,Cu)-rich mixture consistent with a brighter HAADF contrast related to the higher density and average Z of the metal compared to the oxide. The EELS fingerprints of each phase were produced in the same way as for the fresh catalyst. A trivariate histogram (Figure 10Figure 9a) was produced from the elemental maps (**Error! Reference source not found.**Figure 8) and three phases were isolated: the oxides in the light blue circle, the Cu-rich phase in the green triangle and the Cu-Ni-rich phase in the red box. Note that, the oxide composition of the spent catalyst is shifted to Fe-rich composition compared to the oxide of the fresh catalyst (Figure 5Figure 5). The difference is accounted for by the emergence of a Fe-poor metal phase in the spent catalyst (red box) with a concomitant oxygen loss. This is confirmed by the elemental quantification of the spent catalyst (Table 13Table 13). The oxide composition in Fe of the oxide is increased at the expense of the Cu and Ni content.

**Table 13:** Oxide composition of the spent $(Ni_{0.5}Cu_{0.5})Fe_2O_4{}^{MAIN}$ calculated from the EELS reference spectrum.

| Phase | EELS elementals content (%at) | | | |
|---|---|---|---|---|
| | Cu | Ni | Fe | O |
| Oxide | 0.042 | 0.084 | 0.341 | 0.533 |
| Cu-Ni | 0.431 | 0.261 | 0.121 | 0.187 |
| Cu-rich | 0.812 | 0.067 | 0.024 | 0.097 |
| Injected | 0.071 | 0.071 | 0.286 | 0.571 |

From the regions isolated of the trivariate histogram, three reference spectra were produced (Figure 10Figure 9 b – e) with the corresponding color code. The Cu $L_{2,3}$ edge (Figure 10Figure 9 e) of the Cu-rich and the Cu-Ni regions exhibit a metallic signature. The Cu-rich zone is pure and contains trace amounts of O, Fe and Ni, which significantly reduces with the integration region of the trivariate histogram. O and Fe were not found in significant amount in the Cu-NiNi-Cu phase. The shape of the Ni edge ($L_3$ to $L_2$ ratio) of the Cu-NiNi-Cu phase supports the assignment to a metallic state. We then used the reference spectra of (Figure 10Figure 9 b – e) to fit the spectrum image, in which the background prior to the O K edge was removed. This routine produced maps representing the spatial distribution of the isolated phases (Figure 10Figure 9 f). Several maps generated in the same way shows a tendency for the Cu-NiNi-Cu regions to wrap around the Cu-rich zones. This morphology offers an explanation to the abnormally large width of the (002) XRD peak of the previously assigned Cu metal phase (Figure 7Figure 7). TEM analysis confirms the coexistence of a Cu-NiNi-Cu (~1:1) FCC alloy in addition to

pure Cu. A 1:1 Ni-Cu alloy has a 1.5% lattice mismatch, which translates to the addition of another (002) peak, 0.7° away from the Cu (002) peak. Both peaks are assigned to phases having a small crystallite size. Therefore, the overlap of two neighboring broad XRD peaks will naturally lead to the enlargement of that otherwise small XRD peak. Thus, the catalytic reaction conditions caused the disappearance of the Cu(0) clusters to form large Cu-NiNi-Cu rich zones, as well as the extraction of the Cu and the Ni from the $(Ni_{0.5}Cu_{0.5})Fe_2O_4$oxide NPs. We had already identified that Cu(0) species were essential for activity from the comparison of $(Ni_{0.5}Cu_{0.5})Fe_2O_4{}^{MAIN}$ and $(Ni_{0.5}Cu_{0.5})Fe_2O_4{}^{AUX}$ performances (*vide supra*). Based on this, we propose the following deactivation mechanism of the catalyst (Figure 10). First, a fast Oswald ripening occur that change the Cu clusters into larger 20-30 nm Cu particlesNPs. Concomitant to the Oswald ripening, Cu and Ni are extracted from the facetted oxides, which causes the degradation of the crystal lattice, as seen by the porous-like texture (Figure 8Figure 8 a). The Cu and Ni species that jointly act as hydrogen carrier in the "Borrowed hydrogen" process normally reduce the C=N by giving back the hydrogen atom. Notably, the presence of alcohol and *isopropanol* *i*PrOH could act to reduce the ions to their metallic states. This side reaction makes the Cu and Ni atoms adsorbed on the existing Cu particles and form a layer of Cu-NiNi-Cu alloy. Given that no significant leaching is observed, the loss of catalytic activity is thus ascribed to the gradually disappearance of the catalytically active phase of small Cu(0) NPs, in favourfavor of larger particles, and ones covered with a Cu-NiNi-Cu alloy coating.
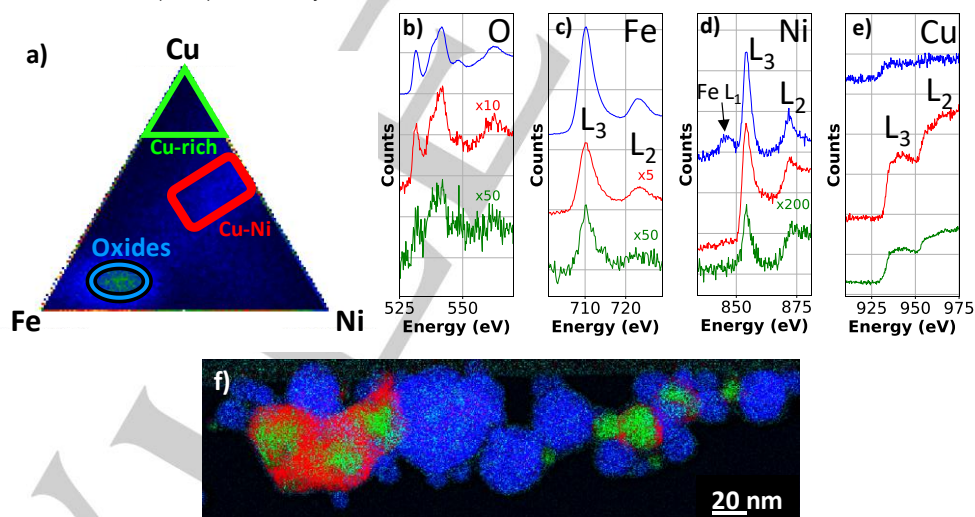


**Figure 9**. a) Trivariate histogram made with the background-subtracted metal edges computed for each pixels of the EELS spectrum images of the spent $(Cu_{0.5}Ni_{0.5})Fe_2O_4{}^{MAIN}$. EELS edges of b) O K c) Fe $L_{2,3}$ d) Ni $L_{2,3}$ e) Cu $L_{2,3}$ of the reference spectra of the phases marked in the trivariate histogram: oxides phase (blue) and the Cu-rich phase (green) and the Cu-NiNi-Cu rich phase (red) f) Fit-coefficient maps of the reference spectra of the oxides (blue), Cu-rich (green) and Cu-NiNi-Cu rich (red) phases.
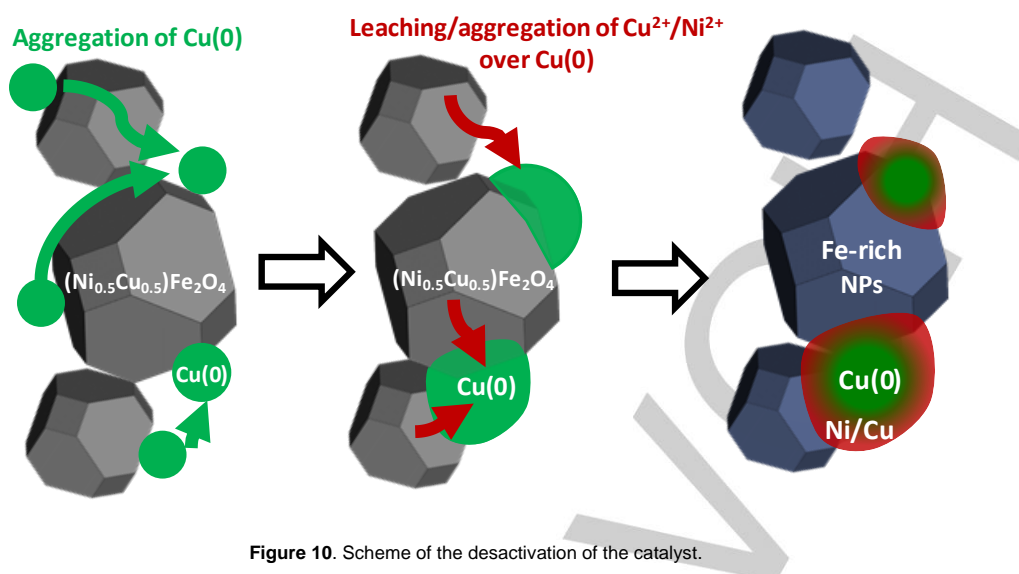
**Figure 10**. Scheme of the desactivation of the catalyst.

## Conclusions

A magnetically recyclable, heterogeneous and noble metal-free $(Ni_{0.5}Cu_{0.5})Fe_2O_4{}^{MAIN}$ catalyst was prepared by RF plasma induction. This technique allowed us to produce well-defined nano-particles at a large scale (c.a. 15 g/h). Detailed analytical TEM characterization demonstrates that this techniques produces facetted Cu,Ni ferrites NPs decorated by finely dispersed metal zero Cu clusters. The catalytic potential of these plasma made NPs for the base-free amination of alcohols was demonstrated. In our case, microwave heating allowed up to a 2.5-fold yield increase compared to oil bath heating, as well as a precise temperature/pressure control. The catalyst was shown to be highly active and re-cyclable up to 6 times. The reaction was easily transposed to the 10 gram-scale, at loadings comparable to that of homogeneous catalyst (up to 2 mol%). Our best turnover (19) surpasses that of heterogeneous Ni/Cu catalysts reported previously. We also provided here an extensive analysis of the active catalysts and the role of each metal in the reaction, thanks for details XRF, XPS, XRD and STEM-EELS analysis. The cause of the catalyst deactivation was then determined to be a loss in specific area due to Oswald ripening of the Cu clusters followed by the Cu and Ni migration from the spinel structure to form a ~~Cu-Ni~~Ni-Cu alloy on the existing Cu particles. Overall, we showed that plasma induction is a potent tool for nanopowder synthesis, ~~with superior catalytic performance in industrially relevant reactions.~~with potential application in organic reactions.

## Experimental Section

### General procedure for catalyst preparation.

The plasma synthesis was conducted using a PL50 model (Tekna Plasma System Inc., 36 kW), connected to RF power supply (3 MHz, Lepel). The synthesis consisted in the coaxial injection of aqueous solution (0.65 mol/L) of $Fe(NO_3)_3 \cdot 9H_2O$, $Cu(NO_3)_2 \cdot 3H_2O$ and $Ni(NO_3)2 \cdot 6H_2O$ in a 4/1/1 molar ratio with a carrier gas into an inductively coupled thermal plasma torch. Prior to injection, the reactor pressure was set to 180 torr. The precursor solution was pumped into a water-cooled gas atomization probe using a peristaltic pump at 5 ml/min. The gases were injected at a controlled rate of 62 slpm of $O_2$ and 5.5 slpm for Ar for the sheath gas, and 10 slpm Ar for the carrier gas. As NPs accumulated on the filters, the pressure increased to 330 torr inside the reactor. After 3 hours 20 min of reaction, the powder was collected separately in the main chamber and auxiliary chamber.

The catalyst characterization was conducted using transmission electron microscopy (TEM), energy dispersive X-ray spectroscopy (EDS) and X-ray fluorescence (XRF).

**Transmission electron microscopy**

NPs were dispersed into EtOH and sonicated. One drop of the NPs EtOH suspension was deposited onto a 200 mesh holey carbon-coated Cu grid and left to dry. The sample was then plasma cleaned at 50 W for 3 minutes. HAADF-STEM images were acquired on a FEI Titan 80-300 equipped with an XFEG source at 200 keV. EELS-STEM were acquired with a Gatan 966 Imge Filter with a convergence angle of 19.1 mrad and a collection angle of 55 mrad.

The elemental quantification of the O, Fe, Ni, Cu content of the oxide reference phase was carried out using the EELS cross-sections calculated from CuO, $Fe_3O_4$ and nickel ferrite standards.[56] Care was taken to position the background window for the extrapolation that avoided the Fe L1 edge (black arrow Figure 5 d).For the TEM images in the SI, samples were deposited on 400 mesh carbon-coated (Lacey) copper grids supplied by Electron Microscopy Sciences. The TEM analyses were performed on the Philips CM200 200 kV TEM, equipped with a AMT XR40B CCD Camera and EDAX Genesis EDS Analysis System.

**X-ray fluorescence**

X-ray fluorescence analysis was acquired with an AXIOS Advanced apparatus by PANalytical. XRF sample first treated with a "loss on ignition'' at 1050°C for 3-4 h step to remove any potential water or organic contamination. Beads were prepared by fusing 0.1000 g of a sample into 0.6 g of a 49.75% $Li_2B_4O_7$, 49.75% $LiBO_2$ and 0.5% LiBr mixture with a THEBEE fluxor from Claisse. Fused beads of WROXI standards from PANanlytical were also prepared with the same procedure to create a calibration curve for many oxides (Na, Mg, Al, Si, O, S, K, Ca, Ti, V, Cr, Mn, Fe, Ni, Cu, Zn, Sr, Zr, Ba, Hf and Pb). Calibration curves were prepared using various concentration and compositions to improve the confidence level and the sensitivity of the technique and to minimize matrix effect.

**X-ray diffraction**

X-ray diffraction analysis was performed on a X'Pert PRO Multipurpose Diffractometer from PANalytical with the Bragg-Brentano geometry and an PIXel1D detector. XRD patterns were collected over a 2θ range of 15° to 108° with a step size of 0.0131° and 2.2 s/step. To remove the fluorescence, the low level of the pulse-height discrimination was raised to 43%.

Rietveld refinement was performed with the PANalytical software HighScore Plus (V3.0.5) using pseudo voigt functions. Theorical X-ray diffraction patterns were modeled with the phases $Cu_{0.5}Ni_{0.5}Fe_2O_4$, CuO, and Cu(0) based on the JCPDF files 04-001-9115, 04-007-1375 and 04-009-2090 from the International Centre for Diffraction Data (ICDD) database. Here, since both $CuFe_2O_4$ and $NiFe_2O_4$ adopt an inverse spinel structure, we considered that every tetrahedral site was occupied with Fe, and that every octahedral site was occupied with a mixture Fe, Cu and Ni. Due to their similar scattering strength, no improvement in the goodness of fit (GOF) was observed when the atomic fraction of Cu, Ni and Fe was changed in the octahedral sites of the spinel and was therefore fixed to the stoichiometry of $(Ni_{0.5}Cu_{0.5})Fe_2O_4$. A significant improvement of the fit was observed when the unit cell parameter and the oxygen displacement (u parameter) were allowed. The scale factor, the unit cell (a0), the Caglioti parameters and the zero shift were refined as shown in Table S1-2 in the supporting information.

All reactants were purchased from Sigma Aldrich and used as received. When relevant, anilines were purified from their oxidation contamination product by vacuum distillation, and stored under argon in a freezer. Unless noted, all catalytic tests were conducted in a Monowave 400 microwave reactor (Anton-Paar), with the glassware (glass or silicon carbide vials) supplied by the vendor.

**Inductively coupled plasma analysis.**

The spent catalyst was rinsed 4 times with acetone and dried overnight in the vacuum oven. The samples were digested in 7 mL of a 6:1 $HCl/HNO_3$ acid mixture (Fisher trace metal grade) in semi-closed HDPE vessels at 90 °C for 6 h. ICP measurements were taken using a Thermo ICP-OES to measure Fe content at the elemental wavelength of 259.940 nm, Ni content at 231.604 nm, and Cu content at 221.810 nm.

**General procedure for alcohol amination.**

In a typical experiment, the amine (1 mmol), alcohol (1.2 mmol), $(Ni_{0.5}Cu_{0.5})Fe_2O_4{}^{MAIN}$ (50 mg, 10 mol% Cu and 10 mol% Ni) and the solvent (*tert*-amyl alcohol (1.8mL) and isopropanol (0.2 mL)) were added to a 5 mL microwave vial equipped with a magnetic stirrer. The vial was purged with Ar for 15 minutes, sealed with a cap and reacted under microwave at 240°C for 60 min, then cooled to RT. Acetone (5 mL) was added to disperse the liquid mixture, which was separated from the catalyst using a strong external magnet. The operation was repeated 3 times, then the mixture was filtered through a pad of Celite. The crude reaction mixture was concentrated in vacuo, and analyzed by NMR, using diphenylmethane as an internal standard.
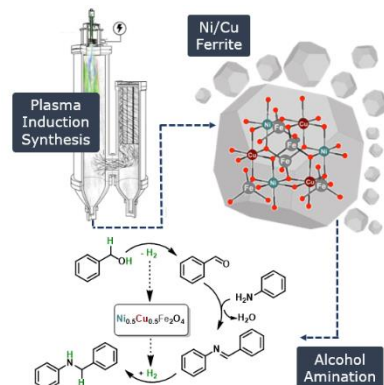
## FULL PAPER

**The three-body solution.** A noble metal-free, magnetically recyclable $(Ni_{0.5}Cu_{0.5})Fe_2O_4$ catalyst was made under plasma conditions. They were shown to catalyze alcohol amination, through a borrowing-hydrogen pathway. The role of each metal in the reaction, as well the mechanism for catalytic deactivation was identified, aided by EELS spectroscopy.

Alain You Li and Nicolas Dumaresq, Andréanne Segalla, Nadi Braidy*, Audrey Moores*

**Plasma-made $(Ni_{0.5}Cu_{0.5})Fe_2O_4$ nanoparticles for alcohol amination under microwave heating**

[1]     S. Bähn, S. Imm, L. Neubert, M. Zhang, H. Neumann, M. Beller, *ChemCatChem* **2011**, *3*, 1853-1864.

[2]     M. Pera‑Titus, F. Shi, *ChemSusChem* **2014**, *7*, 720-722.

[3]     M. Pelckmans, T. Renders, S. Van de Vyver, B. F. Sels, *Green Chem.* **2017**, *19*, 5303-5331.

[4]     Y. Watanabe, Y. Tsuji, Y. Ohsugi, *Tetrahedron Lett.* **1981**, *22*, 2667-2670.

[5]     R. Grigg, T. R. B. Mitchell, S. Sutthivaiyakit, N. Tongpenyai, *J. Chem. Soc., Chem. Commun* **1981**, 611-612.

[6]     G. E. Dobereiner, R. H. Crabtree, *Chem. Rev.* **2010**, *110*, 681-703.

[7]     R. H. Crabtree, *Chem. Rev.* **2017**, *117*, 9228-9246.

[8]     K.-i. Fujita, Z. Li, N. Ozeki, R. Yamaguchi, *Tetrahedron Lett.* **2003**, *44*, 2687-2690.

[9]     O. Saidi, A. J. Blacker, G. W. Lamb, S. P. Marsden, J. E. Taylor, J. M. J. Williams, *Org. Proc. Res. Dev.* **2010**, *14*, 1046-1049.

[10]    A. Corma, J. Navas, M. J. Sabater, *Chem. Rev.* **2018**, *118*, 1410-1459.

[11]    C. Gunanathan, D. Milstein, *Angew. Chem. Int. Ed.* **2008**, *47*, 8661-8664.

[12]    T. Yan, B. L. Feringa, K. Barta, *Nat. Commun.* **2014**, *5*, 5602.

[13]    T. Yan, B. L. Feringa, K. Barta, *ACS Catal.* **2016**, *6*, 381-388.

[14]    T. Yan, B. L. Feringa, K. Barta, *Sci. Adv.* **2017**, *3*.

[15]     S. Elangovan, J. Neumann, J.-B. Sortais, K. Junge, C. Darcel, M. Beller, *Nat. Commun.* **2016**, *7*, 12641.

[16]     S. Rösler, M. Ertl, T. Irrgang, R. Kempe, *Angew. Chem. Int. Ed.* **2015**, *54*, 15046-15050.

[17]     G. Zhang, Z. Yin, S. Zheng, *Org. Lett.* **2016**, *18*, 300-303.

[18]     K.-i. Shimizu, *Catal. Sci. Technol.* **2015**, *5*, 1412-1427.

[19]     R. Cano, D. J. Ramón, M. Yus, *J. Org. Chem.* **2011**, *76*, 5547-5557.

[20]     K.-i. Shimizu, K. Shimura, M. Nishimura, A. Satsuma, *RSC Adv.* **2011**, *1*, 1310-1317.

[21]     K. Shimizu, M. Nishimura, A. Satsuma, *ChemCatChem* **2009**, *1*, 497-503.

[22]     H. Liu, G.-K. Chuah, S. Jaenicke, *J. Catal.* **2012**, *292*, 130-137.

[23]     K. Taniguchi, X. Jin, K. Yamaguchi, N. Mizuno, *Catal. Sci. Technol.* **2016**, *6*, 3929-3937.

[24]     W. He, L. Wang, C. Sun, K. Wu, S. He, J. Chen, P. Wu, Z. Yu, *Chem. Eur. J.* **2011**, *17*, 13308-13317.

[25]     L.-M. Wang, Y. Morioka, K. Jenkinson, A. E. H. Wheatley, S. Saito, H. Naka, *Scientific Reports* **2018**, *8*, 6931.

[26]     S. Furukawa, R. Suzuki, T. Komatsu, *ACS Catal.* **2016**, *6*, 5946-5953.

[27]     H. Chung, Y. K. Chung, *J. Org. Chem.* **2018**, *83*, 8533-8542.

[28]     aR. Martinez, D. J. Ramon, M. Yus, *Org. Biomol. Chem.* **2009**, *7*, 2176-2181; bC. Gonzalez-Arellano, K. Yoshida, R. Luque, P. L. Gai, *Green Chem.* **2010**, *12*, 1281-1287.

[29]     aH. Jinling, Y. Kazuya, M. Noritaka, *Chem. Lett.* **2010**, *39*, 1182-1183; bY. Wu, Y. Huang, X. Dai, F. Shi, *ChemSusChem*, *11*, 1-8.

[30]     M. M. Reddy, M. A. Kumar, P. Swamy, M. Naresh, K. Srujana, L. Satyanarayana, A. Venugopal, N. Narender, *Green Chem.* **2013**, *15*, 3474-3483.

[31]     P. R. Likhar, R. Arundhathi, M. L. Kantam, P. S. Prathima, *Eur. J. Org. Chem.* **2009**, *2009*, 5383-5389.

[32]     H. Yang, X. Cui, X. Dai, Y. Deng, F. Shi, *Nat. Commun.* **2015**, *6*, 6478.

[33]     C. F. Winans, H. Adkins, *J. Am. Chem. Soc.* **1932**, *54*, 306-312.

[34]     aA. Tomer, F. Wyrwalski, C. Przybylski, J.-F. Paul, E. Monflier, M. Pera-Titus, A. Ponchel, *J. Catal.* **2017**, *356*, 111-124; bK.-i. Shimizu, N. Imaiida, K. Kon, S. M. A. Hakim Siddiki, A. Satsuma, *ACS Catal.* **2013**, *3*, 998-1005; cK.-i. Shimizu, K. Kon, W. Onodera, H. Yamazaki, J. N. Kondo, *ACS Catal.* **2013**, *3*, 112-117.

[35]     Y. Qi, H. Yu, Q. Cao, B. Dong, X. Mu, A. Mao, *Catalysts* **2016**, *6*, 63.

[36]     A. Y. K. Leung, K. Hellgardt, K. K. M. Hii, *ACS Sustainable Chem. Eng.* **2018**, *6*, 5479-5484.

[37]     E. Denkhaus, K. Salnikow, *Critical Reviews in Oncology/Hematology* **2002**, *42*, 35-56.

[38]     M. Imabeppu, K. Kiyoga, S. Okamura, H. Shoho, H. Kimura, *Catal. Commun.* **2009**, *10*, 753-757.

[39]     aH. Abe, Y. Yokota, K. Okabe, *Appl. Catal.* **1989**, *52*, 171-179; bH. Kimura, K. Matsutani, S.-i. Tsutsumi, S. Nomura, K. Ishikawa, Y. Hattori, M. Itahashi, H. Hoshino, *Catal. Lett.* **2005**, *99*, 119-131.

[40]     X. Cui, X. Dai, Y. Deng, F. Shi, *Chem. Eur. J.* **2013**, *19*, 3665-3675.

[41]     aM. Y. Malca, H. Bao, T. Bastaille, N. K. Saadé, J. M. Kinsella, T. Friščić, A. Moores, *Chem. Mater.* **2017**, *29*, 7766-7773; bM. J. Rak, N. K. Saadé, T. Friščić, A. Moores, *Green Chem.* **2014**, *16*, 86-89; cM. J. Rak, T. Friščić, A. Moores, *RSC Adv.* **2016**, *6*, 58365-58370.

[42]     U. R. Kortshagen, R. M. Sankaran, R. N. Pereira, S. L. Girshick, J. J. Wu, E. S. Aydil, *Chem. Rev.* **2016**, *116*, 11061-11127.

[43]     E. V. Shunko, D. E. Stevenson, V. S. Belkin, *IEEE Transactions on Plasma Science* **2014**, *42*, 774-785.

[44]     D. Vollath, *KONA Powder and Particle Journal* **2007**, *25*, 39-55.

[45]     I. Mohai, L. Gál, J. Szépvölgyi, J. Gubicza, Z. Farkas, *J. Eur. Ceram. Soc.* **2007**, *27*, 941-945.

[46]     aS. Bastien, N. Braidy, *J. Appl. Phys.* **2013**, *114*, 214304; bS. Bastien, C. Ricolleau, N. Braidy, *Plasma Chem. Plasma Proc.* **2016**, *36*, 1349-1362.
[47]     L. Jia, F. Gitzhofer, *Plasma Chem. Plasma Proc.* **2009**, *29*, 497.
[48]     aN. Kaloglu, I. Özdemir, N. Gürbüz, M. Achard, C. Bruneau, *Catal. Commun.* **2016**, *74*, 33-38; bX. Xie, H. V. Huynh, *ACS Catal.* **2015**, *5*, 4143-4151.
[49]     T. A. Geissman, in *Organic Reactions* (Ed.: J. W. Sons), **2011**.
[50]     R. D. Patil, S. Adimurthy, *Asian. J. Org. Chem.* **2013**, *2*, 726-744.
[51]     J. D. Hayler, D. K. Leahy, E. M. Simmons, *Organometallics* **2019**, *38*, 36-46.
[52]     aD. Obermayer, B. Gutmann, C. O. Kappe, *Angew. Chem. Int. Ed.* **2009**, *48*, 8321-8324; bJ. M. Kremsner, C. O. Kappe, *J. Org. Chem.* **2006**, *71*, 4651-4658.
[53]     aM. Lukasiewicz, D. Bogdal, J. Pielichowski, *Adv. Synth. Catal.* **2003**, *345*, 1269-1272; bD. Bogdal, M. Lukasiewicz, J. Pielichowski, A. Miciak, S. Bednarz, *Tetrahedron* **2003**, *59*, 649-653.
[54]     A. de la Hoz, Á. Díaz-Ortiz, A. Moreno, *Chem. Soc. Rev.* **2005**, *34*, 164-178.
[55]     I. Polaert, S. Bastien, B. Legras, L. Estel, N. Braidy, *J. Mag. Mag. Mater.* **2015**, *374*, 731-739.
[56]     R. F. Egerton, *Electron energy-loss spectroscopy in the electron microscope*, Springer Science & Business Media, **2011**.